

Supporting Information

Discovery of SIAIS178 as an effective BCR-ABL degrader by recruiting von Hippel-Lindau (VHL) E3 Ubiquitin Ligase

Quanju Zhao^{‡#∇}, Chaowei Ren^{‡†∇}, Linyi Liu^{‡#∇}, Jinju Chen[‡], Yubao Shao[&], Ning Sun^{‡#}, Renhong Sun^{‡#}, Ying Kong[‡], Xinyu Ding[‡], Xianfang Zhang[‡], Youwei Xu[‡], Bei Yang[‡], Qianqian Yin^{‡*}, Xiaobao Yang^{‡*}, Biao Jiang^{‡§*}

[‡]Shanghai Institute for Advanced Immunochemical Studies, [†]School of Life Science and Technology, ShanghaiTech University, Shanghai, 201210, China.

[#]Shanghai Institutes for Biological Sciences, Chinese Academy of Sciences, Shanghai, 200031, China.

[&]Department of Histology and Embryology, Anhui Medical University, Hefei, 230032, China

[§]CAS Key Laboratory of Synthetic Chemistry of Natural Substances, Shanghai Institute of Organic Chemistry, Chinese Academy of Sciences, 345 Lingling Road, Shanghai 200032, China

*Corresponding authors.

Email: jiangbiao@shanghaitech.edu.cn; yangxb@shanghaitech.edu.cn;
yinqq@shanghaitech.edu.cn

[∇]These authors contributed equally to this work.

Contents of Supporting Information:

Figure S1. A suitable site for attaching to VHL ligand for the design of potential PROTACs according to the co-crystal structure of c-ABL complexed with dasatinib.

Figure S2. **19** retains potency and selectivity against the BCR-ABL driven cell lines.

Figure S3. **19** significantly reduced protein levels BCR-ABL and downstream signaling.

Figure S4. GST-pull down assay in the presence of **19**.

Figure S5. The comparison of binding affinity with ABL kinase and cell permeability.

Figure S6. The kinase profile and proteomic analysis of the degrader **19**.

Table S1. Pharmacokinetic Properties of **19** in Rats

Figure S7. The dose-dependent efficacy of the degrader **19** in murine xenograft model of K562 cells *in vivo*.

Figure S8. The degradative activity of degrader **19** against clinically relevant mutations.

Figure S9. ¹H NMR spectrum of compound **19**.

Figure S10. HPLC analysis of compound **19**.

Scheme S1. The synthesis of compound **7** (DAS-6-2-2-6-VHL)

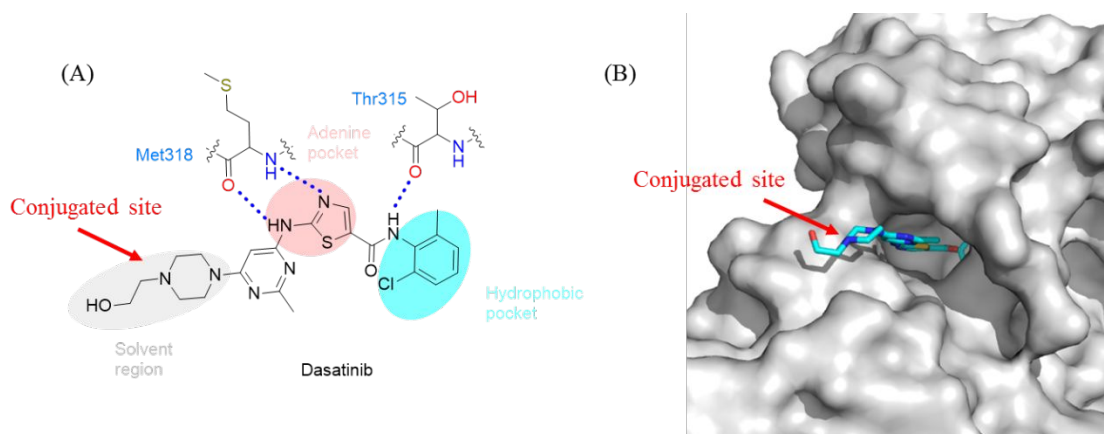


Figure S1. Co-crystal structure of c-ABL complexed with dasatinib (PDB code 2GQG) and conjugated site for attaching to VHL ligand. (A) The binding mode of dasatinib with BCR-ABL; (B) The orientation of dasatinib in BCR-ABL ATP pocket.

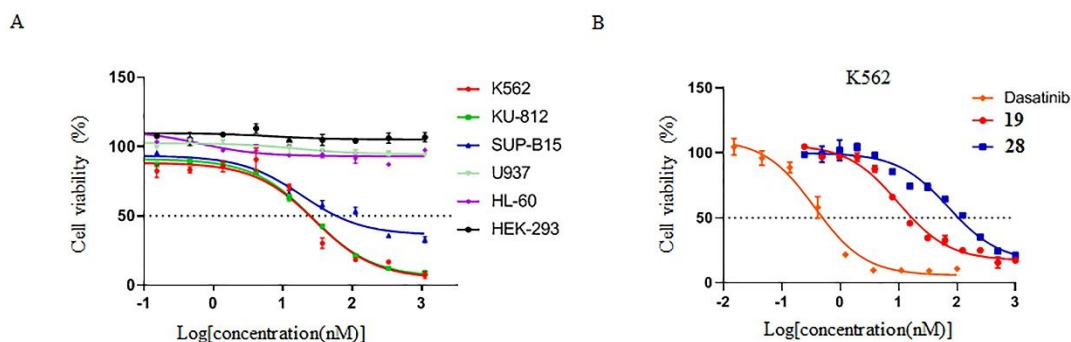


Figure S2. **19** retains potency and selectivity against the BCR-ABL driven cell lines. (A) Effect of compound **19** BCR-ABL-driven and non BCR-ABL-driven cell lines. (B) Effect of compound **19**, **28** and dasatinib on K562 cells.

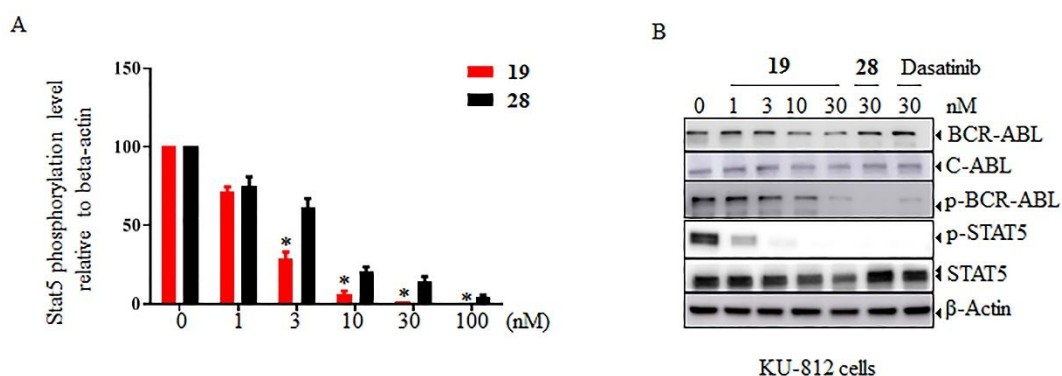


Figure S3. **19** significantly reduced protein levels of BCR-ABL and downstream signaling. (A) The quantification of p-STAT5 in K562 cells following treatment of **19** and **28**. The symbols * indicate $P < 0.05$ compared with the **28**-treated samples. (B) KU-812 cells were treated for 16 h with **19** and **28** as well as Dasatinib. Cell lysates were collected and analyzed by immunoblotting using Abs against the indicated proteins. Data are representative of three independent experiments.

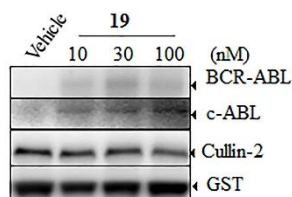


Figure S4. GST-pull down assay in the presence of **19**. K562 cell lysate was incubated with vehicle or different dosing of **19** in the presence of excess immobilized GST-VBC bait. The beads were washed and bound proteins eluted with SDS buffer and analyzed by western blot. Cullin-2 were included as the positive control, which interacted with VHL endogenously.

Affinities for the ABL kinase domain ^a			Mean Papp (10 ⁻⁶ cm/s)		
Compound	ABL (non-phosphorylated)	ABL (phosphorylated)	Compound ID	A to B	B to A
Dasatinib	0.032	0.029	Dasatinib	3.18	8.85
19	0.35	0.14	19	0.02	0.07
28	0.53	0.35	28	0.01	0.09
DAS-VHL (8)	0.33	0.1	DAS-VHL (8)	0.14	1.30

^a Kd affinity values in nM

Figure S5. The comparison of binding affinity with ABL kinase and cell permeability. (A) The binding affinities (Kd) to phosphorylated and non-phosphorylated c-ABL kinase domain were determined with compounds as indicated using the KinomeScan platform *in vitro*. (B) Permeation of the test compounds from A to B direction or B to A direction in Coca-2 was determined.

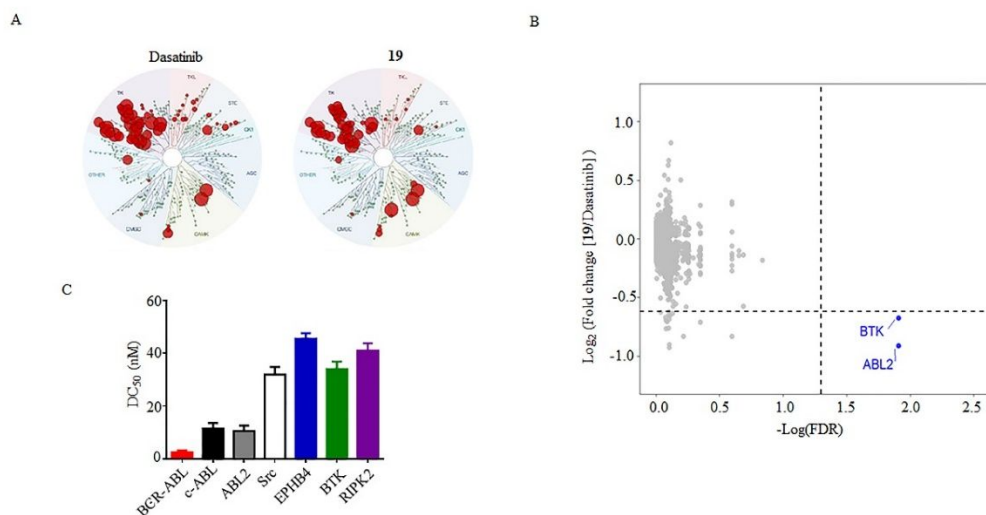


Figure S6. The kinase profile and proteomic analysis of the degrader **19**. (A) The kinase profile of dasatinib and the degrader **19** on 468 human kinases (KINOMEScan). Compounds were tested at 1 μ M concentration. Bound kinases are indicated by red circles of size proportional to the percentage of binding to each kinase. A target is considered to bind to the compound with its percent of control less than 35%. (B) K562 cells were treated with either **19** or dasatinib at 100 nM concentration for 16 hours. The proteins were labeled with tandem mass tags and the global proteomic alterations was assessed by multiplexed tandem mass spectrometry. Quantification of 8,201 proteins was analyzed according to Methods. Dasatinib was included as a negative control to exclude proteins which is down-regulated because of transcriptional regulation or destabilization by the inhibitor alone. Protein abundance is normalized to vehicle and dasatinib-treated control groups. Dotted lines at y axis indicate the cutoff for a protein to be degraded (protein abundance is below 65% via dasatinib-treated samples). Dotted lines at x axis indicate the False discovery rate (FDR)-adjusted p values P-values (x axis) below 0.05 were considered as significant. The protein level reducing below 65% via control group in paralleled with a false discovery rate of less than 5% was considered as the target of our PROTAC (blue dotted). (C) The DC₅₀ value of proteins indicated in Figure 6B were calculated through the western-blot image.

Table S1. Pharmacokinetic Properties of 19 in Rats

parameter	unit	IV dose (2 mg/kg)	IP dose (2 mg/kg)
$T_{1/2}$	h	3.82	12.35
T_{max}	h	0.083	9
C_{max}	nM	1165.2	30.0
$AUC_{(0-t)}$	h*nM	426.1	307.4
$MRT_{(0-\infty)}$	h	2.24	16.3
CL	mL/h/kg	4821.8	NA

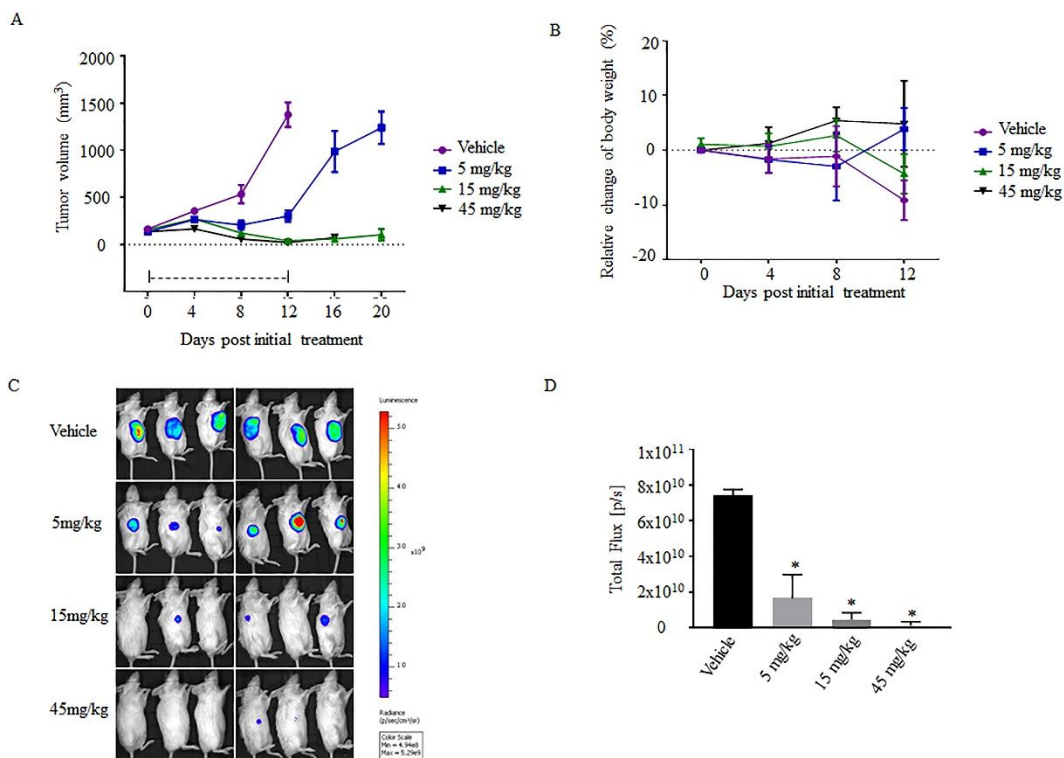


Figure S7. The dose-dependent efficacy of SIAIS178 (**19**) in murine xenograft model of K562 cells in vivo. (A) The tumor volume was measured following treatment of **19** at different dose-schedules. The dashed-line indicate the treatment period. (B) The body weight alteration was measured following treatment of **19** at different dose-schedules. (C) Tumor burden was monitored by measuring the luciferase activity through bioluminescence imaging; (D) Quantitative results were analyzed for six mice of each group and expressed as total photon values per second (Total Flux [p/s]). The symbols * indicate $P < 0.05$ compared with the vehicle-treated samples.

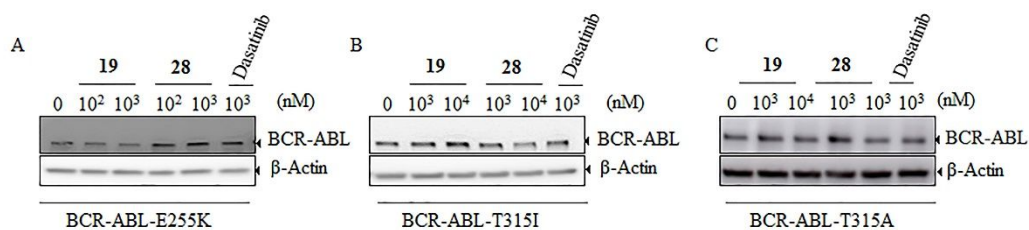


Figure S8. The degradative activity of degrader **19** against clinically relevant mutations. Blotting analysis of compounds **19** in U937 exogenously expressing clinically relevant mutations of BCR-ABL as indicated.

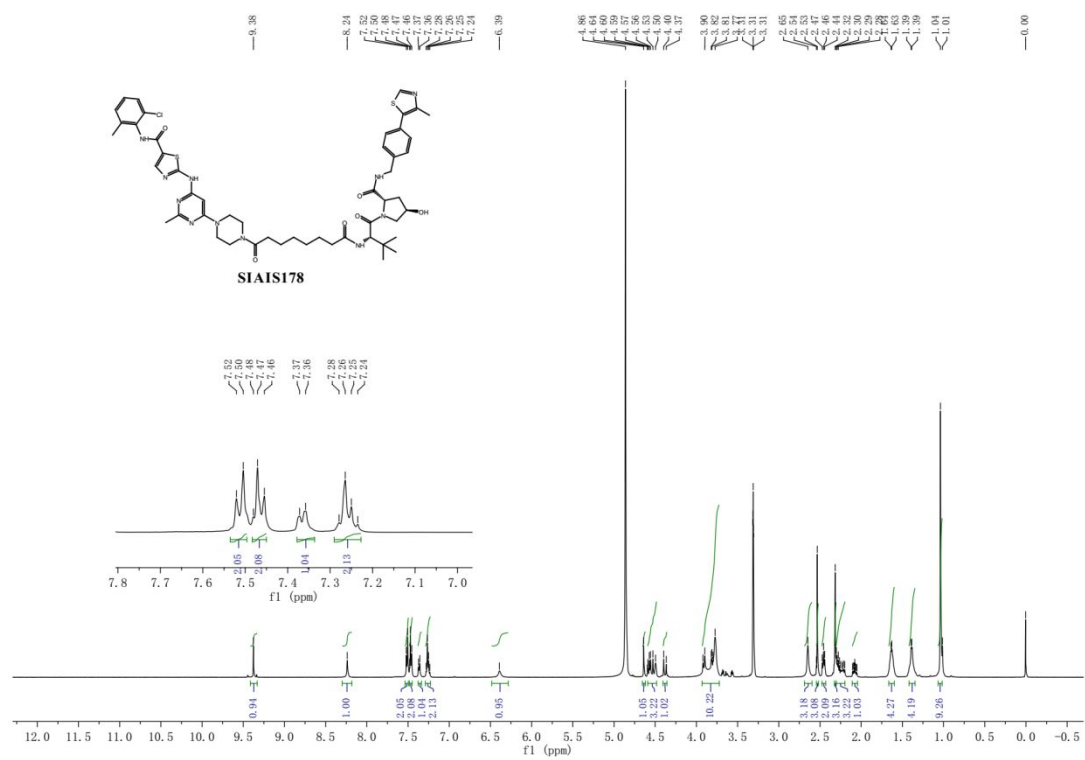
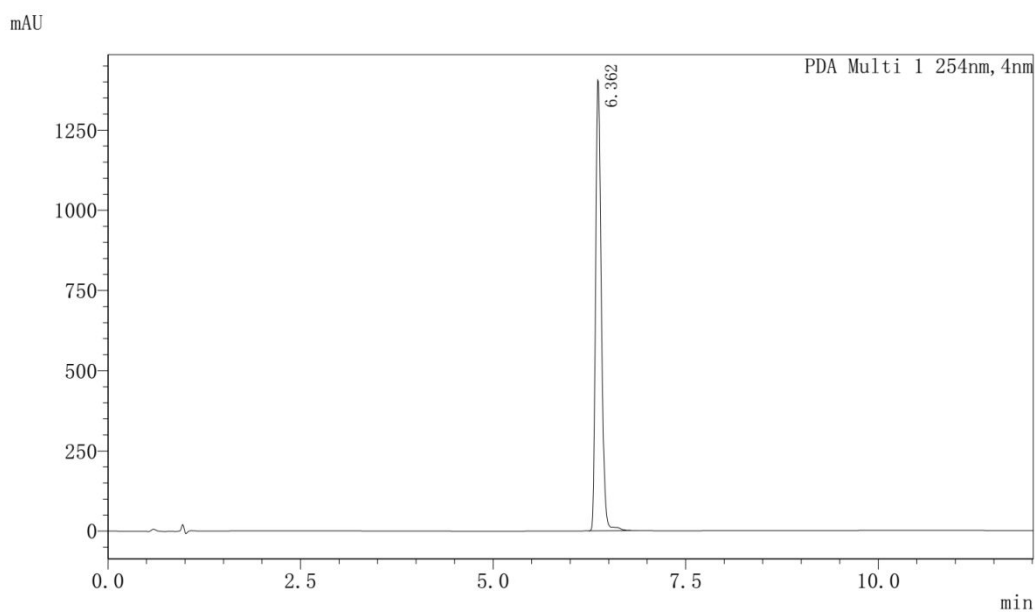
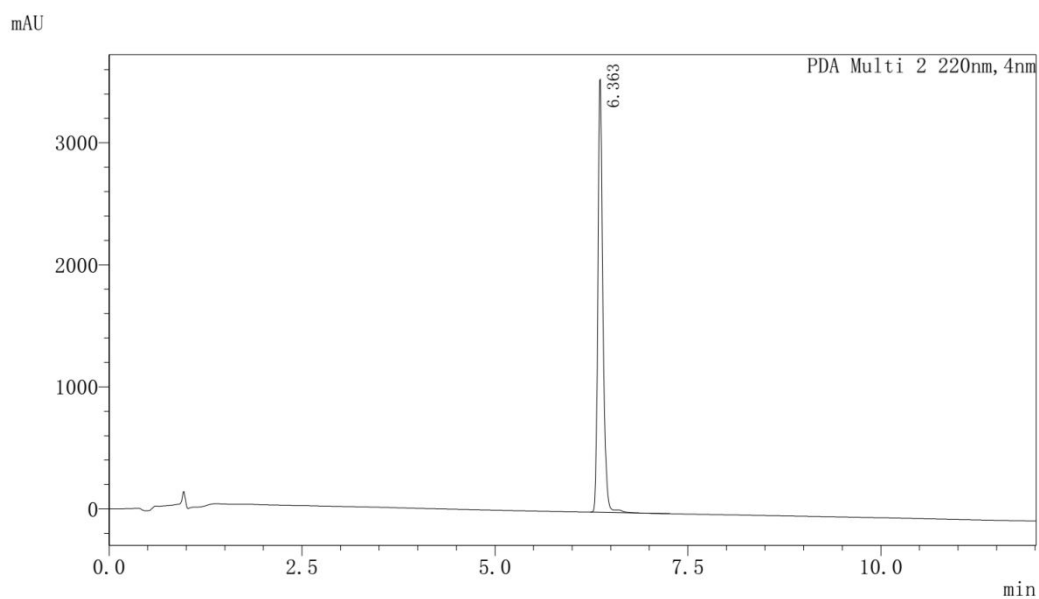


Figure S9. ¹H NMR spectrum of compound 19.



PDA Ch1 254nm

	Retention time	Area	Height	Area%	USP	tailing factor
1	6.362	7251169	1404946	100.00	28663	1.286
Total		7251169	1404946	100.00		



PDA Ch1 220nm

	Retention time	Area	Height	Area%	USP	tailing factor
1	6.363	15981106	3548024	100.00	40759	1.254
Total		15981106	3548024	100.00		

Figure S10. HPLC analysis of compound **19**.

Scheme S1. The synthesis of compound 7 (DAS-6-2-2-6-VHL)

